https://doi.org/10.15407/ufm.24.03.530

**M.A. LATYPOVA[1,*], S.L. KUZMIN[2,**], and A.S. YERZHANOV[1,***]**

[1] Karaganda Industrial University,
Republic Ave., 30, Temirtau, 101400 Kazakhstan

[2] Rudny Industrial Institute,
50 let Oktyabrya Str., 38, 111500 Rudny, Kazakhstan

* m.latypova@tttu.edu.kz, ** info@rii.kz, *** a.yerzhanov@tttu.edu.kz

# INFLUENCE OF SELECTIVE LASER MELTING PROCESS PARAMETERS ON THE MICROSTRUCTURE FORMATION

Additive technologies for making products by laser melting of powders have been rapidly developed recently. However, such technologies impose increased requirements on the properties of alloys used for the manufacturing of parts. Laser-melting technologies are a promising direction in the development of metal products due to several advantages, such as (1) the possibility of manufacturing complex-shaped parts with internal cavities and thin partitions; (2) significant material savings due to the precise manufacturing of part of a given shape according to a computer model that does not require the use of subsequent conventional turning, milling, and cutting operations; (3) achieving a higher level of mechanical properties due to increased cooling speeds compared to standard technologies by means of the formation of a more dispersed structure.

**Keywords:** additive technologies, powder metallurgy, selective laser melting, microstructure, microstructure control, heat treatment.

## 1. Introduction

Additive manufacturing has immense prospects for development in the medical, automotive, aerospace, and foundry industries and is currently a global manufacturing trend. Selective laser melting (SLM) is one of the new methods of additive manufacturing that uses high-power lasers

Citation: M.A. Latypova, S.L. Kuzmin, and A.S. Yerzhanov, Influence of Selective Laser Melting Process Parameters on the Microstructure Formation, *Progress in Physics of Metals*, **24**, No. 3: 530–560 (2023)

(usually ytterbium fibre lasers) to create three-dimensional physical objects by fusing metal powders. The essence of selective laser fusion technology consists of the layered manufacture of a part, where the heat source is laser radiation. Selective laser melting, as one of the additive manufacturing technologies, 'prints' materials and components directly from the computer-aided design file, thereby offering unique advantages of design freedom for complex parts without the need for moulds. Since SLM is a layer-by-layer build-up technology, it provides ample opportunities to adjust the microstructure, and then mechanical properties. The development of additive technologies, in particular the technology of selective laser melting, makes it possible to manufacture metal products of complex geometric shapes, the production of which by traditional methods is often not viable. SLM is a multi-factor technology: the structure and properties of the resulting products depend on a large number of initial parameters. Their variation affects the structure, porosity, and, therefore, the properties of the alloy by setting the energy contribution, the volume of molten metal in the manufacturing process, *etc.* It is necessary to understand the regularities of the influence of a particular parameter on the final result to control the technological process. Recently, works have been presented in the literature investigating the relationship between the parameters of manufacturing products by selective laser melting, and the structure and properties of the resulting material. Nevertheless, little information has been published about the possibility of using the features of the selective laser melting process to specify the crystallographic texture and grain size of alloys, and even less information about the relationship between the preferred anisotropy, microstructure, and mechanical properties of the alloy.

The main factors determining the use of lasers are their low divergence (laser show, laser pointer, audio player), the purity and coherence of their spectrum (pollution detection, length/velocity measurement, interferometry, *etc.*), or a combination of all factors (communication, holography, metrology). As a result, many lasers have been created capable of producing a wide range of wavelengths, energy, time/spectral distribution, and efficiency [1–3]. The continued growth of laser technologies in the processing of materials is explained by several unique advantages of lasers: high productivity, non-contact processing, lower processing costs, increased material utilization, suitability for automation, exclusion of finishing operations, improved product quality, and a small area of thermal influence.

From a practical point of view, there are four main categories of laser processing of materials: mechanical processing (cutting, drilling, *etc.*) and connection (welding, soldering, and surface treatment (processing is limited only to the near-surface area) [4–6]

One of the latest applications of laser processing is the development of small and complex components by integrating a laser with computer-aided design and computer-controlled positioning stages. This technology is based on layer-by-layer processing of the material and repeated deposition, known as the additive manufacturing method of arbitrary shape.

## 2. Application of Laser Technology

The dependence of the methods of laser processing of materials on the interaction time and laser power (power density) is shown in Fig. 1 [7]. Technological processes can be divided into three main classes: heating (without melting/evaporation), melting (without evaporation), and evaporation. The interaction time/pulse time and the laser power density are selected in each case so that the necessary phase transitions occur in the processed material depending on the heating degree. There are two degrees of power density: low and high. The low specific power of the laser makes it possible to carry out processes without melting the surface: bending, quenching, and magnetization control. High power density, which involves melting, corresponds to such processes as welding, glassmaking, cutting, surface melting, and surfacing. Drilling, cutting, and similar machining processes remove the material in the form of steam therefore an extremely high power density distribution over a short interaction/pulse time is required.

As shown in Fig. 2, *a*, the $CO_2$ laser device consists of three main parts: an amplification medium or laser, an optical resonator or resonator with two mirrors, and an energy source or pump that supplies energy to the laser. The chemical appearance in the amplification medium determines the wavelength of optical radiation between two mirrors. One of the mirrors is fully reflective, and the other is partially reflective. According to the quantum-mechanical principle, when external energy is supplied to the atom, the irradiated atom reaches an excited state (Fig. 2, *b*). This phenomenon is known as spontaneous emission (Fig. 2, *c*). A spontaneously emitted photon can, in turn, excite another atom and induce it to emit a photon, transferring it to a lower energy level. This process is called stimulated emission of radiation (Fig. 2, *c*). A photon interacting with an unexcited atom can be absorbed by it and excite it to a higher energy state. This process called 'population inversion' is created by the pumping source. Photons moving along the optical axis interact with a variety of excited atoms, stimulate them, and are thereby amplified. They are reflected from the resonator mirrors and pass through the excited medium, creating even more photons. In each circular journey, some of these photons exit through a partially transmitting mirror in the form of an intense laser beam (Fig. 2, *d*).

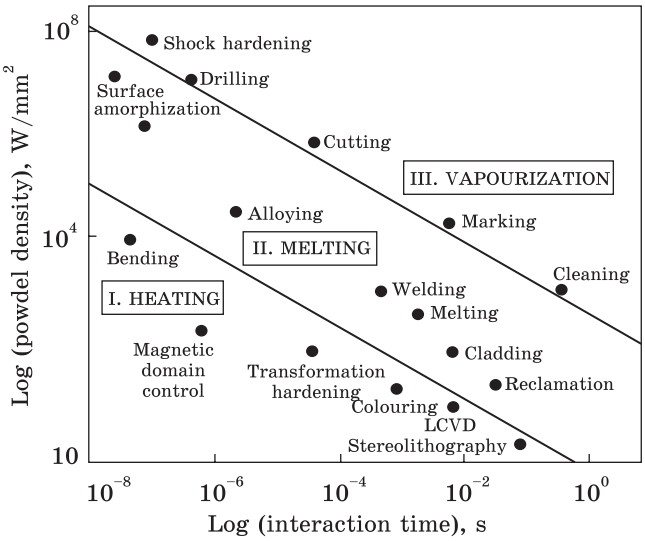


*Fig. 1*. Diagram in terms of laser power density as a function of interaction time for different laser material treatment processes [7]

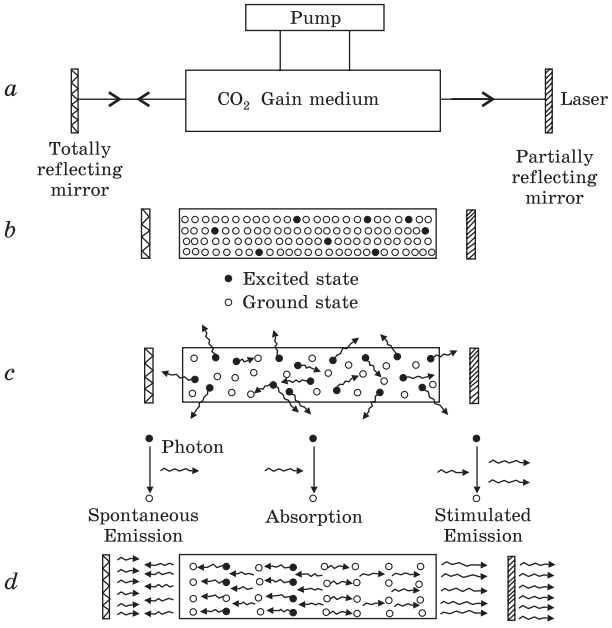


*Fig. 2*. Schematic illustration of a continuous laser installation: (*a*) the instruments that make up the laser, (*b*) the first stage of laser operation, (*c*) excitation of atoms in the medium that leads to laser emission, (*d*) formation of the laser beam [7]

Finally, the laser beam is either directed to the work piece using reflective mirrors or delivered to the desired location *via* an optical fibre [7].

The advantage of these methods is the production of parts of complex shapes with high precision, fast processing time, no physical tool, no processing effort or tool wear, saving material and energy consumption, *etc.* [8–10]. On the other hand, the main obstacles that limit the use of lasers for processing various materials are high initial capital and

maintenance costs, additional components, as well as the need for skilled labour, and the impossibility of using the process for heat-sensitive materials, for example, such as aluminium laminated structures with fibreglass.

However, the features associated with laser radiation impose several restrictions on materials suitable for such technologies. Firstly, alloys should have a low tendency to form defects under laser exposure (crystallization cracks, pores, oxide films); have high corrosion resistance concerning account operating conditions; have stable properties under various types of load (static, dynamic).

## 3. Materials Used in Laser Processing

Well-established metals used in laser processing are alloys based on iron, titanium, and nickel [11] due to their traditional use and ease of processing. Iron-based alloys have been studied since 1993 [12] and are currently the most commonly used since they are easy to process and have a low cost. Nickel-based alloys are the basis for many heat-resistant superalloys, so they are preferred as materials for aerospace engines. Titanium-based alloys are widely used in medicine due to their satisfactory biocompatibility [11]. The theoretical density of these materials is of 4.51 $g \cdot cm^{-3}$ for titanium, of 7.83 $g \cdot cm^{-3}$ for iron, and of 9.81 $g \cdot cm^{-3}$ for nickel. Light structural metals such as magnesium with a density of 1.74 $g \cdot cm^{-3}$ and aluminium with a density of 2.7 $g \cdot cm^{-3}$ cannot be successfully processed by laser melting without reducing their mechanical properties. Thus, there are intense problems with the use of alloys based on these metals [13].

Numerous attempts have been made to process magnesium and magnesium alloys [14] but small progress has been achieved in the development of alloys from such materials with the desired set of properties [15]. The main problem with processing such materials is the tough evaporation of magnesium during processing. Magnesium has a melting point of 650 °C and a relatively low boiling point of 1093 °C compared to aluminium, which has a boiling point of 2470 °C and a melting point of 660 °C. Doping is one of the methods that can be used to eliminate such a problem [16]. In addition, this may increase the gas pressure, but excessive evaporation of Mg is still a problem and may affect the final properties of the product [17].

One of the most promising alloys for laser melting is aluminium. Some aluminium alloys, especially Si-alloyed alloys, beyond alloys with other additives, have been thoroughly investigated in recent years. [18]. The main limitations of SLM processing are the formation of oxides, high reflectivity, poor wetting, low melt viscosity, and poor powder flowability [19]. To deal with these problems, powerful lasers were

used to increase the temperature of the melt bath, thus it was possible to improve the structure by eliminating surface oxides and improving wetting. Various aluminium alloys are currently being processed. A new task for many researchers is an attempt to process aluminium alloys hardened by aging, which will be used as a structural material in low-weight structures [18]. The main problem of all heat-strengthened aluminium alloys is that they tend to form hot cracks during crystallization and require special heat treatment to obtain the necessary microstructure [13]. During selective laser melting, tough crystallization cracks of aluminium alloys were recorded, and the main goal is to identify the cause of their formation to find ways to eliminate them [20–22].

Laser melting technologies are based on the processes of melting small volumes of metal during the operation of a high-energy source. Due to the admission of a laser as an energy source, a unique thermal regime is created, characterized by small volumes of the melt bath and high cooling rates equal to $10^4$–$10^6$ K/s [23]. Due to this, the structure formed in the resulting products is characterized by high dispersion of the solid solution and excess phases and, as a result, a higher level of mechanical properties. However, as the practice has shown, the structure of such products is highly heterogeneous in volume: the size and shape of grains and excess phases can vary greatly from layer to layer. As a rule, it consists of alternating zones of columnar and equiaxed crystals [24, 25]. Different sizes and shapes of the structural components indicate different conditions for the crystallization of small volumes of the melt. One of the essential advantages of additive technologies over traditional technologies is the control of the structure of products from layer to layer. A lot of publications are devoted to this issue. Scientists propose various methods that boil down to varying the technological parameters of the process, such as reducing the anisotropy of the structure by alternating the scanning path of the laser beam from layer to layer, heating the substrate to reduce the temperature gradient at the melt/metal interface, which reduces the directional heat dissipation and, as a consequence, the number of zones of columnar crystals [26, 27]. However, the described methods do not thoroughly solve the problem of microstructure heterogeneity.

Thus, the enhancement of new alloys for additive technologies is an urgent task. The most promising materials for additive technologies may be aluminium alloys with transition metals and modifying additives. However, the need to obtain special powders from experimental alloys and the high cost of 3*D* printers complicate the process of developing such materials. In this regard, an urgent task is to improve a methodology that allows analysing the behaviour of alloys

under laser processing conditions, beyond evaluating the tendency of alloys to form various defects with minimal time and material costs, while obtaining results reproducible in additive manufacturing conditions.

The materials used in SLM processes are subject to requirements for granulometric composition, particle shape and geometry, the ability to absorb and reflect laser radiation, and indeed such properties as weldability. These materials include stainless steels (17-4PH, 15-5PH, 316L), tool steels (1.2709, 1.2344), cobalt–chromium alloys ($CoCr_{28}Mo_6$), titanium alloys ($Ti_6Al_4V$), nickel alloys (IN625, IN718, IN939), aluminium alloys ($AlSi_{12}$, $AlSi_7Mg_{0.6}$, $AlSi_9Cu_3$). At the same time, the powders used should have a fraction from 20 to 60 μm and a ratio that would provide the necessary filling density.

## 4. Role of Parameters on the Microstructure Formation

Laser melting and additive technologies are based on high-energy laser or electronic sources similar to traditional fusion welding technologies. Due to this, the structure of products obtained using additive technologies is consistent with the structure of welded joints. [28–30]. However, additive technologies have a significant advantage, namely, the possibility of layer-by-layer control of the structure of products by regulating the melting conditions and crystallization of the melt bath. The structure control parameters during laser melting are most often understood as all parameters affect the temperature gradient, the cooling rate, and the direction of heat removal during crystallization [28]. These include scanning speed, laser energy, spot size, powder particle size; powder feed rate (for direct laser melting technology), layer thickness, and scanning trajectory [31]. Several technological parameters can affect the manufacturing process and, consequently, the quality of the final product. Among other things, parameters such as laser power, laser scanning speed, laser spot size, scanning distance and trajectory, and beyond layer thickness are the most important factors that strongly influence the final result [32].

The relationship between the distance between the tracks in the hatching, the laser scanning speed, and the relative density of the SLM samples are shown in Fig. 3 at a constant laser power of about 200 W and a layer thickness of 40 microns. While the scanning speed increases in all four cases, the relative density drops significantly. Figure 4 shows a comparison of the microstructure of the cross-section obtained at different scanning speeds. That confirms the results in Fig. 3 that a higher scanning speed leads to a relatively lower density. With a lower scanning speed, the size of the defects de-

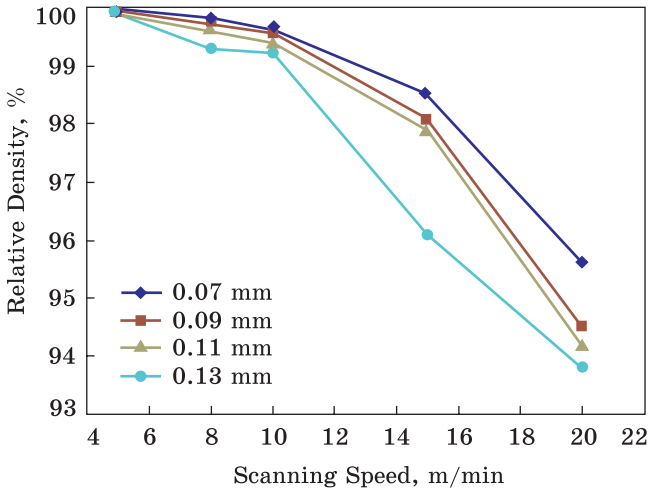


*Fig. 3*. Graph of the effect of track spacing in the hatch and scanning speed on relative density at constant laser power [33]

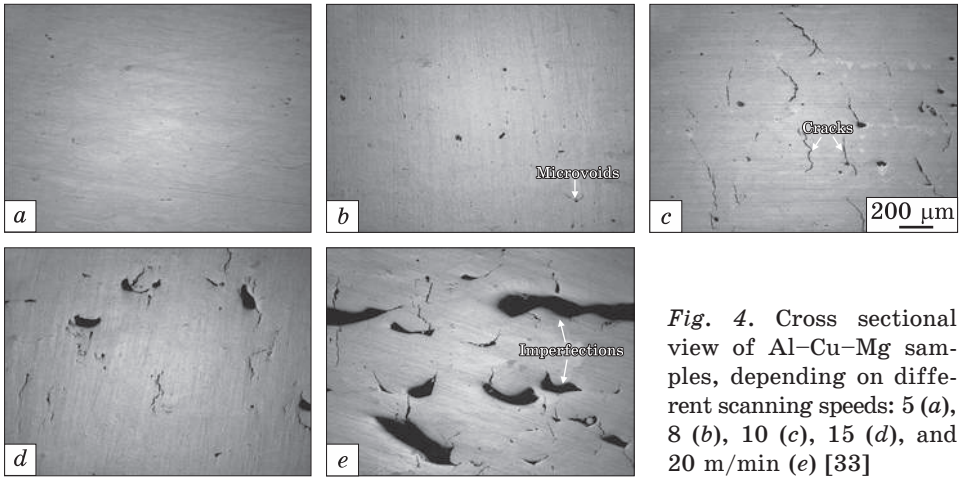


*Fig. 4*. Cross sectional view of Al–Cu–Mg samples, depending on different scanning speeds: 5 (*a*), 8 (*b*), 10 (*c*), 15 (*d*), and 20 m/min (*e*) [33]

creases, which means that the density increases. In addition to defects, crystallization cracks were also obtained due to the high sensitivity of Al–Cu–Mg alloys to cracking. That is because alloying elements in the Al–Cu–Mg alloy (such as Cu and Mg) lead to a relatively wide effective crystallization interval (ECI) compared to binary alloys and, accordingly, increase the potential for cracking. When the scanning speed decreases from 20 m/min to 8 m/min, defects and microcracks disappear, but microvoids are still detected in the microstructure. All this indicates that the compaction behaviour of SLM samples strongly depends on the energy used [33].

The modes of laser melting and additive technologies depend on the ratio of two parameters: the duration of interaction and the energy

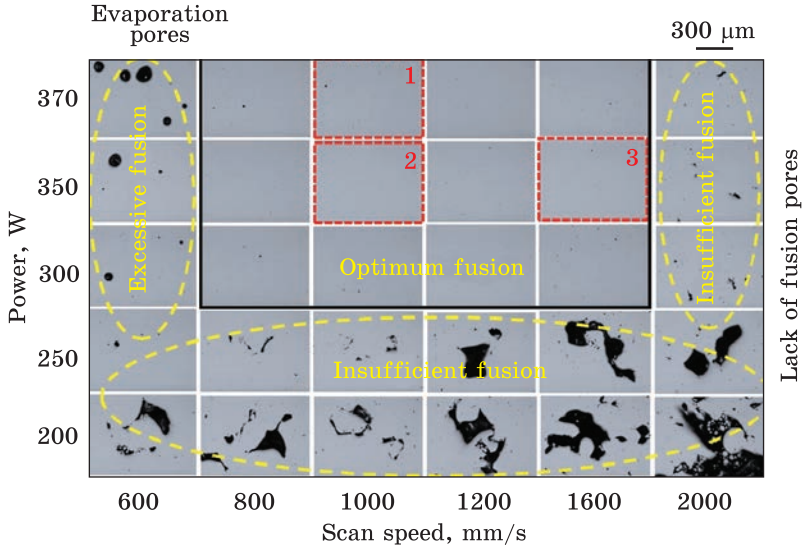


*Fig. 5*. Microstructure images of AlMnMgScZr samples showing porosity at different laser powers and scanning speeds. The area highlighted with a solid black frame shows the optimum processing window [34]

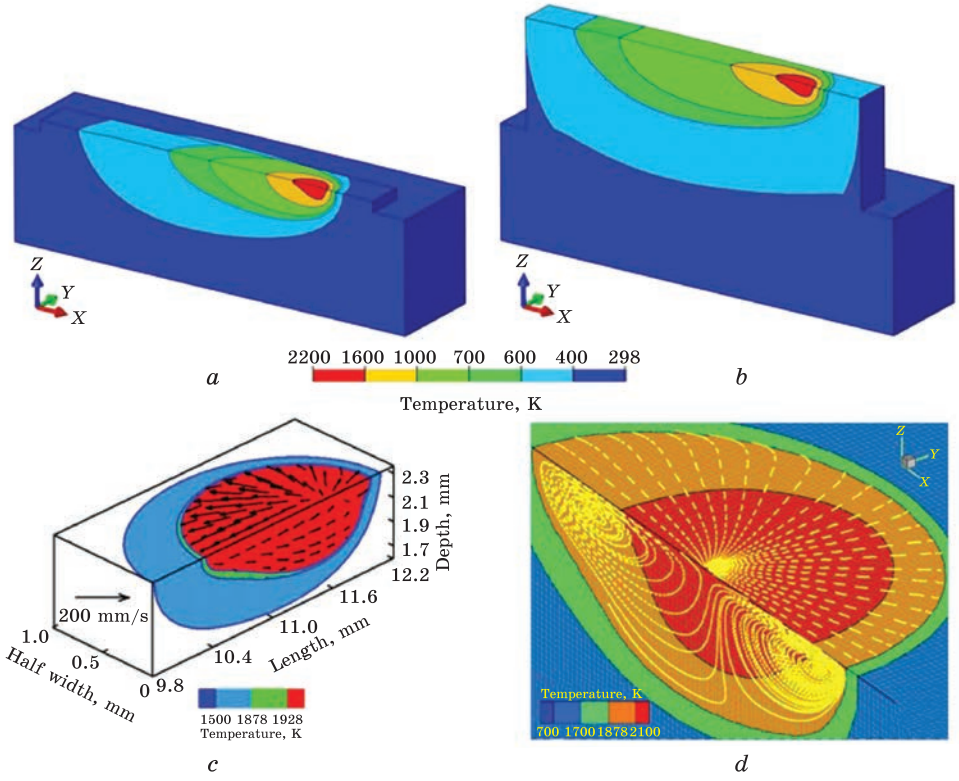


*Fig. 6*. Temperature distribution during direct laser spraying of the 1st (*a*) and 10th layers of steel powder IN 718 (*b*) onto the substrate IN 718 at a power of 300 W and a scanning speed of 15 mm/s (scanning direction along the abscissa axis). (*c*) The shape and size of the melt bath in 10th layer. (*d*) The circulation of molten metal in the molten bath [42]

density of the laser beam. Energy density is an important parameter that shows how much energy is needed to melt a definite metal volume.

Laser power and scanning speed affect the number, size, and morphology of pores (Fig. 5). The images show that with a constant laser power of 200 W or 250 W, irregular pores gradually appear. They are formed when the laser power and scanning speed exceed 300 W and 1600 mm/s. Their formation is due to the low energy of the laser, as a result of which melting does not occur. A low scanning speed of 600 mm/s causes typical evaporation pores at 300 W or higher due to excessive reflow during welding. These pores have a diameter of more than 100 microns and are almost circular. At a flow rate of more than 600 mm/s, the number and size of these pores decrease, and only a few little rounded pores with a size of fewer than 100 microns are observed. In this range of scanning speeds, it is possible to obtain samples with a high degree of consolidation and without significant defects, as shown in Fig. 5 [34].

The analysis of melt crystallization conditions during selective laser melting is a difficult task. In Refs. [35–37], a method of temperature control using a thin thermocouple fixed at a certain distance from the melt is described. This research method allows you to accurately determine the heating temperature of the substrate/layer at various distances from the melt and obtain information about the magnitude and direction of heat removal. In studies [38–41], the method of infrared thermography is used to measure the temperature distribution. However, this method does not allow for analysing the temperature distribution in the volume. These papers describe both methods of temperature measurement (examples of calculating the temperature gradient at the melt/solid metal interface) and the cooling rate. However, there is no information about the relationship of these data with the structure of specific alloys. Figures 6, *a* and *b* show the calculated temperature distribution for the $1^{st}$ and $10^{th}$ layers during direct laser sintering of steel powder IN 718 [42]. Different colours reveal different temperatures. In laser processing, heat dissipation is carried out through the substrate/crystallized layer; thus, with continuous melting of several layers, heat dissipation is reduced by heating the substrate. Figure 6, *c* shows the calculated shape and size of the melt bath when surfacing the $10^{th}$ layer. Inside the melt bath, the maximum temperature is in the centre, and the minimum temperature is at the melt/solid metal interface. The inhomogeneous temperature distribution leads to a gradient of surface tension. Figure 6, *e* shows that the flow of molten metal is controlled by the gradient of surface tension inside the molten bath. Possible crystallization options were discussed in detail in the article [43].

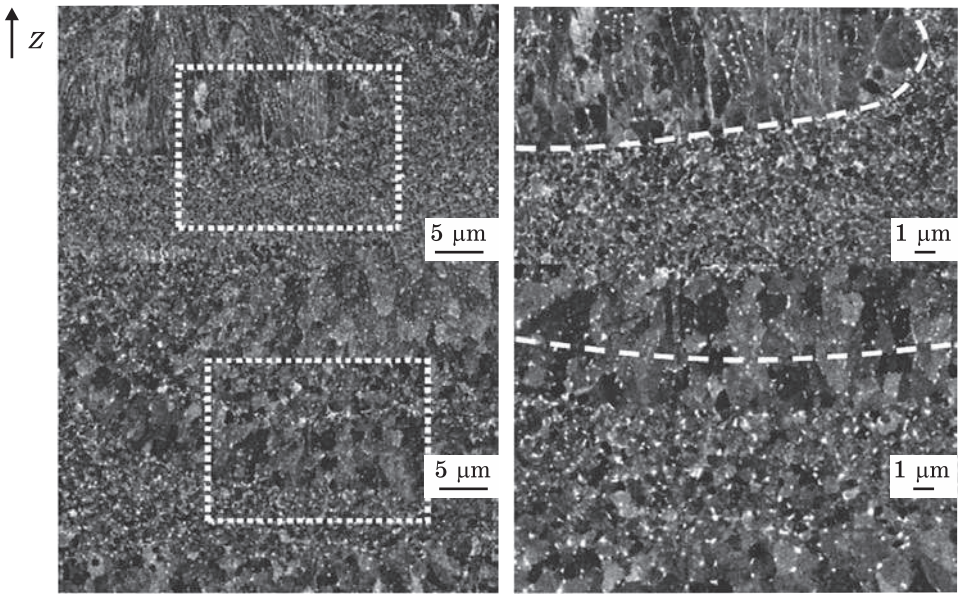


*Fig. 7.* Photos of AlMgScZr alloy microstructure, where (*a*) and (*b*) fabricated at platform temperature of 35 °C, (*c*) and (*d*) fabricated at platform temperature of 200 °C [45]

As is known, the direction of crystal growth depends on the temperature gradient, the influence of the geometry of the melt bath, and the welding speed on the formation of hot cracks, as a result of which the crystal structure was classified. Increasing the welding speed changes the direction of dendrite growth towards the middle of the melt bath. Consequently, the fusible phases are concentrated in the middle of the melt bath, and the tendency to hot cracking increases. A further increase in the welding speed leads to an equiaxed dendritic crystal growth in the centre and a uniform distribution of fusible phases, which reduces the tendency to form hot cracks [44]. The emergence of hot fissures is influenced by temperature gradients, the geometry of the melt bath, and cooling conditions. Changing the welding speed is not the only way to control the geometry of the melt bath and cooling conditions.

When the laser is applied to the powder layer, it heats up from the surface to the substrate. Figure 7 shows SEM images of the AlMgScZr alloy obtained at $E$ = 77 J/mm$^3$. In the overlap zone of the two laser scanning paths, small equiaxed grains are formed, and columnar grains grow from the bottom of the melt bath to its centre. The frequency of remelting of the overlap area depends on the scanning method and processing parameters. Small equiaxed grains are formed mainly along the remelting regions due to the high concentration of $Al_3$(Sc, Zr) nuclei. A positive temperature gradient from the remelting area to the upper part

of the melt bath promotes grain growth during crystallization [45]. The grains grow in the direction of the centre of the melt bath, where the degree of supercooling is greater and the number of embryos is smaller. If the samples are made at a temperature of 35 °C and 200 °C, the number of columnar grains is significantly less at 200 °C than at 35 °C. It is also worth noting that the size of the equiaxed grain when using a temperature of 35 °C is larger (Fig. 7, *e*) than at 200 °C (Fig. 7, *b*): the average size of the equiaxed grain for samples made at 35 °C is approximately 70 nm, and the grain size at 200 °C (Fig. 7, *b*) is 1.19. nm. With a decrease in the cooling rate and temperature gradient, the area with equiaxed grains grows at a platform temperature of 200 °C. That makes it possible to obtain an almost thoroughly equiaxed grain structure.

One of the critical problems of laser melting is the formation of an inhomogeneous structure and, as a consequence, the appearance of anisotropy of properties, which, along with crystallization cracks and porosity, refers to the principal defects of laser melting [46]. The problem of the porosity of the samples obtained by selective laser melting is the subject of most studies. According to the shape and size of the pores, porosity is divided into two categories: gas porosity, which is the result of the absorption of gases (N, O, or H) by the melt or evaporation of alloying elements (Mg, Zn), and porosity due to incorrectly selected parameters of selective melting [46]. It has been found that the most significant effect on the porosity of products is exerted by the laser scanning speed and its power [47–50]. Most of the research is devoted to optimizing the energy density parameter. Porosity occurs at low energy density due to the incomplete melting of metals due to insufficient laser radiation energy; gas porosity occurs at high energy density. In this case, the gas in the protective chamber is captured by the flow of molten metal, or hydrogen is formed due to the evaporation of bound water from the oxide film during melting. Therefore, to reduce porosity, the laser melting process is optimized for each alloy separately, taking into account the properties of alloying components, material properties, and the type of protective atmosphere [51].

The second significant defect is the formation of hot cracks. The reasons for their occurrence are substantially the same as in melting welding: a wide effective crystallization interval and low plasticity in a brittle temperature range. However, additive technologies should also consider the presence of a rigid thermal cycle with high heating and cooling rates, accompanied by the appearance of a large temperature gradient and the formation of an inhomogeneous structure. In this case, the presence of columnar crystals in the structure may have a negative effect. The causes of hot cracks are discussed in more detail below. In studies devoted to additive technologies [52–55], the main reason for the formation of hot cracks is a wide effective crystallization interval. The most common way to solve this problem is to increase the amount of eutectic and, as a rule, we are talking about adding more alloying

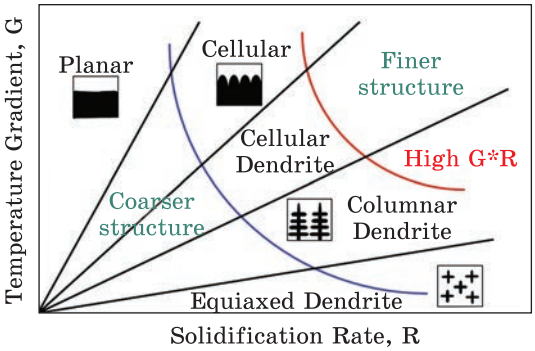


*Fig. 8.* Influence of temperature gradient $G$ and phase growth rate $R$ on the morphology and size of the structural components of aluminium alloys [60, 61]

elements to high-strength alloys of the Al–Zn–Mg–Cu system, grinding grain, as well as transition elements, silicon, and others [56, 57].

As noted above, the grain structure depends on the melting and crystallization conditions of the melt bath. As a rule, the nucleation of solid phases occurs at the melt/solid metal boundary, followed by epitaxial growth. The preferred direction of extension of crystallizing phases is parallel to the heat sink; therefore, crystals with a crystallographic orientation favourable for extension are strongly elongated in one direction and form a columnar structure [58, 59]. The paper [60] describes the evolution of the morphology of alloy 6082 grains during the solidification of a molten bath during argon-arc welding. The simulation considered heat transfer, the flow of liquid metal in the molten bath, and the crystallization parameters. The calculated ratio of the local temperature gradient to the crystallization rate was used to simulate the growth of columnar and equiaxed grains during solidification. The simulation results show that columnar grains are formed at a low scanning speed of 2 mm/s. The transition from the columnar type of crystals to the equiaxed one is observed at a speed of 8–11.5 mm/s. Figure 8 shows a diagram describing the effect of the temperature gradient $G$ and the growth rate $R$ on the microstructure of aluminium alloys. The microstructure can be columnar, cellular, and equiaxial. Whereas Fig. 9 shows a schematic diagram of grain distribution by morphology for a $T$-shaped compound, the effect of the temperature gradient $G$ and the growth rate $R$ on the morphology and grain size during solidification, and the effect of supercooling of the structure on grain morphology [61, 62].

The main features of aluminium alloys in fusion welding are their high reflectivity and high thermal conductivity. Therefore, for melting small volumes, it is necessary to apply such an amount of energy to take into account the losses on reflection and heat generation. For joining various parts made of aluminium-based alloys, the

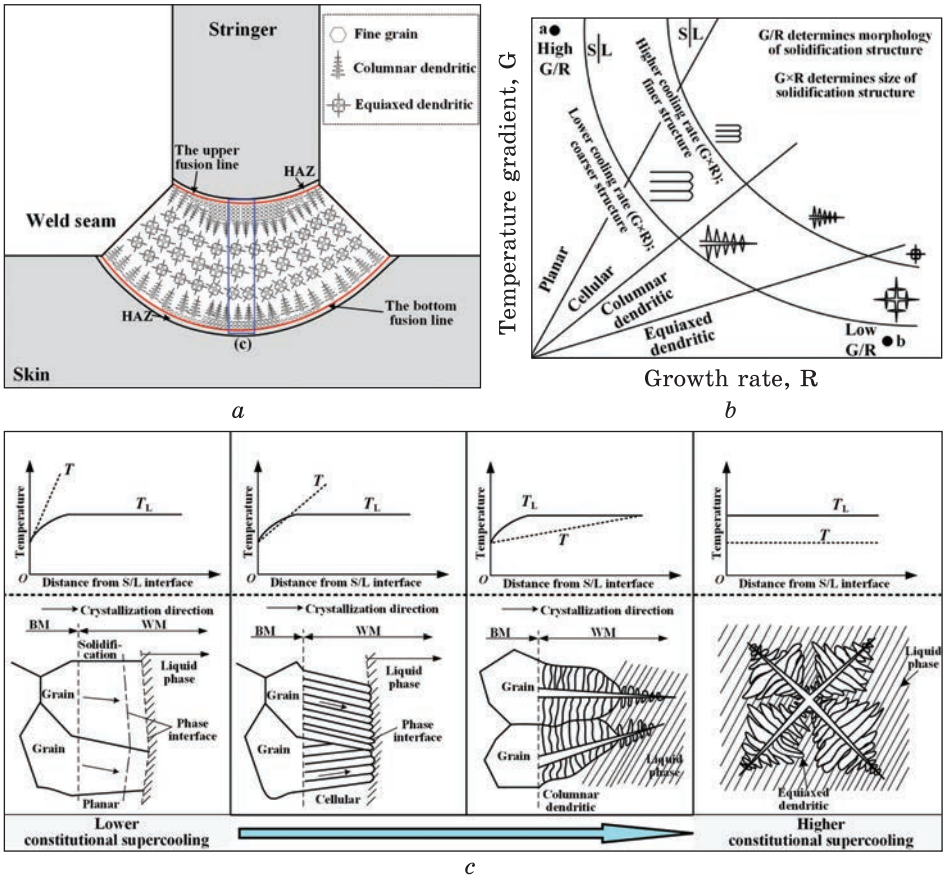


*Fig. 9.* (*a*) The schematic diagram of grain morphology distribution for the *T*-joint. (*b*) Effect of temperature gradient *G* and growth rate *R* on the grain morphology and size during the solidification process. (*c*) Effect of constitutional supercooling on grain morphology. Here, HAZ denotes the heat-affected zone, WM is the weld metal, BM is the melted base metal, *T* is the crystallization temperature curve, $T_L$ is the liquidus temperature curve [62]

following methods of fusion welding have long been known: oxygen–acetylene welding, carbon electrode welding, manual arc welding with a melting electrode, automatic submerged arc welding, manual argon-arc welding with a tungsten electrode, automatic welding with a tungsten electrode, automatic and semi-automatic welding with a melting and non-melting electrode [63].

All of the above methods of fusion welding of aluminium alloys have a large number of disadvantages and are currently limited in use or are not used. For example, during arc welding of aluminium alloys in inert gases, the following defects occur: gas porosity (48%), oxide films (32%) and tungsten inclusions (12%) [64]. Also, the main

disadvantages of these methods include heavy contamination of the seam metal with flux residues, which causes metal corrosion; low process productivity; coarse-grained structure obtained during the crystallization of a large-volume melt bath; high requirements for the preparation of the metal to be welded and the filler material. Some of the difficulties in arc welding can be overcome with the help of special technological operations in complex alloyed additive materials, physical impact on the melt bath, subsequent heat treatment, *etc.* All this complicates and increases the cost of manufacturing technology.

The use of a laser beam for welding aluminium alloys has significant advantages over arc welding [65] adduced below.

• A high concentration of energy and a small heating area makes it possible to obtain a small melt bath compared to arc welding, which has a positive effect on the product characteristics. Reducing the size of the melt bath and obtaining seams with a large ratio of the depth of the melting area to the width can reduce the deformation of parts by about 10 times, which saves metal by reducing the size of the tolerance. The small size of the molten metal and the specific shape of the seam occasionally improve the crystallization conditions and, thereby, the properties of welded joints.

• High productivity due to the laser speed, which is several times higher than the speed of arc welding, saves time for editing after processing. In addition, post-welding treatment can be excluded.

• The absence of an electrode near the welding bath protects the treated area from foreign elements.

• A rigid thermal cycle with high heating and cooling rates can significantly reduce the near-shock zone, preventing phase and structural transformations in the near-shock area, leading to softening, reduced corrosion resistance, *etc.* [65].

In the article [65], the influence of the thermal effect of laser radiation during the welding of heat-strengthened alloys AD37, B-1424, and B96C is investigated. After welding of these materials, due to phase and structural transformations, their softening is observed in the seam area and near-seam zone. Parameters such as the shape and size of the melt bath, the temperature at the points closest to the seam (near-seam area), the residence time of the metal at these points at specified temperatures, and the crystallization and cooling rate of the bath were evaluated.

Since laser welding has a large number of advantages over other types of welding listed above, laser radiation has been used as a source of high energy for the manufacture of various products made of promising aluminium, titanium, and iron alloys [66–71] using additive technologies. The weldability of aluminium alloys depends on their tendency to form hot cracks, so not all known alloys belong to the group of wel-

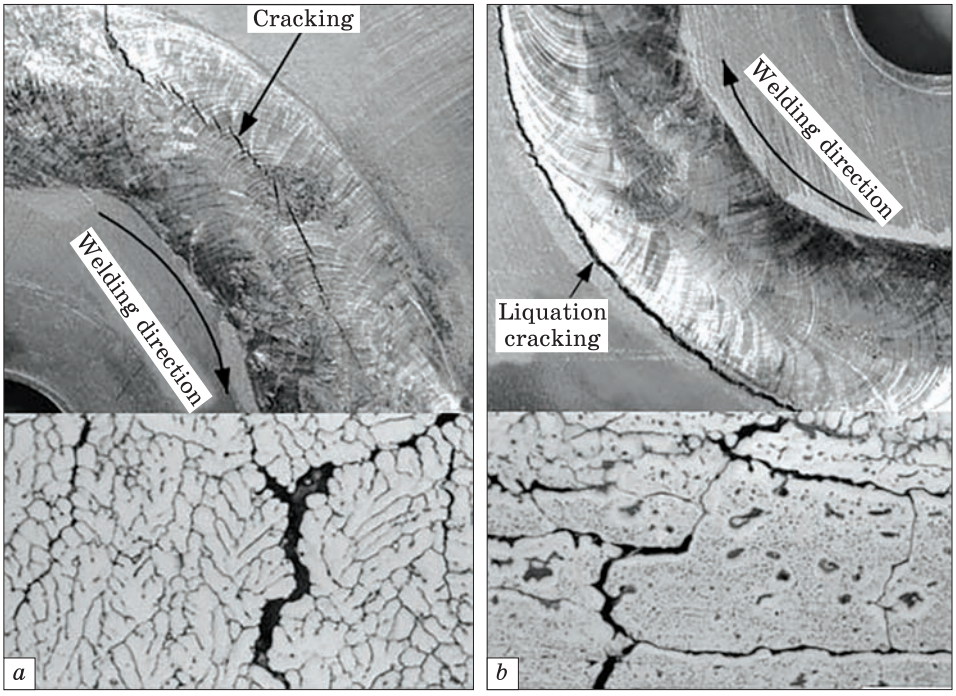


*Fig. 10*. Optical microscopy microstructure images show two types of cracks: (*a*) crystallization cracks and (*b*) liquation cracks [67]

dable. The tendency of aluminium alloys to hot cracking depends on the magnitude of the effective crystallization interval (ECI) and plasticity in the brittle temperature range [72].

During laser welding and melting of aluminium alloys, two types of cracks may form; crystallization fissures may form in the melting (fusion) zone (FZ), and liquation cracks may form in the partial melting zone (PMZ). Figure 10 shows examples of liquation cracking and crystallization cracking in annular seams of aluminium alloys. As can be seen, crystallization cracks occur along the central line of the weld, while liquation cracking occurs along the outer edge of the weld. When processing the alloy, the melt bath is surrounded by a semi-solid metal [73]. Cracking during crystallization is caused by the formation of intercrystallite fissures, as shown in Fig. 10, *a*. The dendritic structure of the solidifying metal is often revealed on the fracture surface. That indicates that the formation of hot cracks during crystallization occurs near the end of the solidification process when the dendrites have almost completely turned into grains separated by a small amount of liquid in the form of films along the grain boundaries. At this stage, the weld metal is susceptible to tensile stresses/deformations causing cracking. Tensile stresses/deformations can occur in the weld

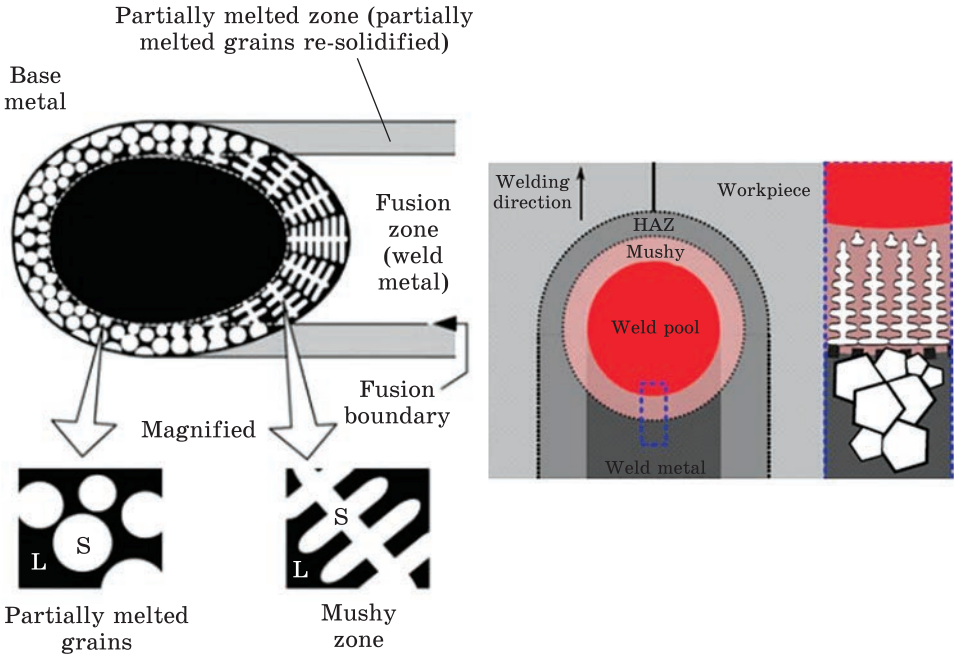


*Fig. 11*. A diagram showing partially molten grains of the base metal and a mushy zone around the alloy welding bath during welding (*e.g.*, ring welding), where *S*, *L*, and HAZ denote the base-metal grains, the intergranular liquid, and heat-affected zone, respectively [73, 74]

metal if it cannot freely compress during cooling, as in a highly constrained work piece, for example, when welding with annular surfacing (Fig. 10). Due to shrinkage during solidification and thermal compression, the seam metal is compressed during cooling [73], which leads to the formation of fissures.

Figure 11 shows the zones formed during welding; the boundary of the molten bath is at the liquidus temperature of the weld metal. The mushy zone, consisting of dendrites (*S*) and interdendritic fluid, is located behind the welding bath (*L*). Fusion zone (FZ) or weld metal (WM) is a thoroughly solidified material. A semi-solid zone consisting of partially molten metal grains (*S*) and intercrystallite liquid (*L*) is located on the sides and in front of the molten bath. Behind, the partially molten grains on the walls of the bath is a thoroughly solidified material called the PMZ. Here, the temperature is higher than the eutectic temperature of the base metal.

The effective crystallization interval, the amount and distribution of liquid at the final stage of crystallization, the primary crystallizing phase, the grain boundary surface tension of the liquid, the plasticity of the crystallizing weld metal, the grain structure and the

tendency to shrink the weld; all these factors can affect the tendency of the weld to crack during crystallization. The first two parameters depend on the microsegregation during solidification, which in turn can be affected by the cooling rate. In some cases, the cooling rate also affects the primary crystallizing phase (for example, regarding austenitic stainless steel). Crystallization cracks of Al and its alloys are primarily associated with the content of alloying elements, just as in steel alloys, the formation of cracks during fusion welding proceeds according to the same principle, depending on the composition of the alloy, as the formation of cracks during casting [75]. The value of the ECI, *i.e.*, the interval between the temperature of the beginning of linear shrinkage and the solidus temperature of the system increases with an increase in the content of the second component, passes through the maximum, and decreases to zero in eutectic systems [71].

It has been shown that molten zones with smaller equiaxed grains are less sensitive to crystallization cracking in aluminium alloys. Small equiaxed grains can deform efficiently by compression stresses, so they are more ductile. Crack healing and fluid delivery can also be more effective in the fine-grained alloy. In addition, since the grain boundary region is much larger in fine-grained material, the emissions with low melting points are less concentrated along the grain boundaries. On the other hand, the tendency of PMZ to liquation cracking can be influenced by the grain structure, the degree of liquation, shrinkage of the seam metal, plasticity in the hot state, and the level of restriction. The degree of liquation in PMZ is determined by the susceptibility of the material to liquation and the amount of heat supplied. The susceptibility of aluminium alloy to liquation increases as the temperature range of solidification and the proportion of liquid during crystallization increase. Alloy 7075, for example, melts much better than alloy AA6061, because it has a wider ECI and a larger amount of liquid during crystallization. Liquor cracking can be controlled by selecting the base metal whenever possible.

The use of fine-grained materials helps to reduce liquor cracking due to a lower concentration of secretions, which cause liquor and higher plasticity. Cast materials are particularly susceptible to liquation cracking due to the presence of fusible phases along grain boundaries. During welding in PMZ, strong liquation of grain boundaries can occur that makes them very susceptible to liquation cracking. Examples are cast 304 stainless steel and cast corrosion-resistant austenitic stainless steel. Liquation cracking can be reduced by heat treatment of castings before welding using homogenization [76].

A small amount of silicon (Si) can lead to grain growth in traditional castings by 2:3 wt.%. As a result, the mechanical properties of

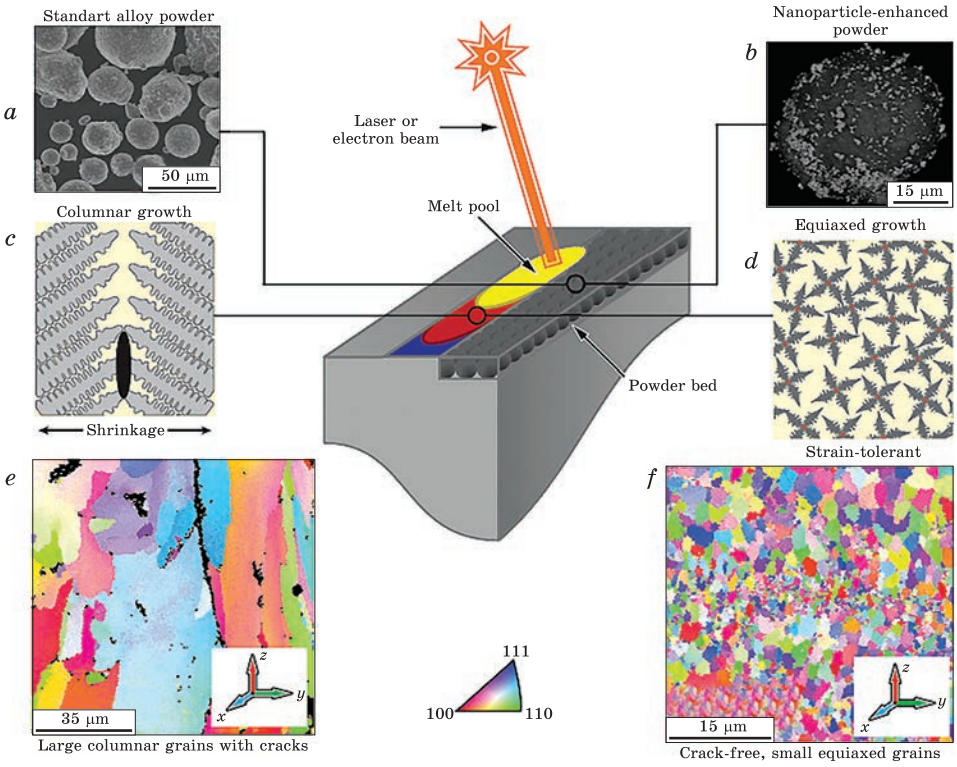


*Fig. 12.* (Colour online) Central schematic showing an overview of an additive manufacturing process in which a direct energy source melts a layer of metal powder (yellow) which solidifies (red to blue) by fusing with a previous layer of metal (grey). (*a*) Standard raw material in the form of AA7075 alloy powder. (*b*) AA7075 powder, functionalized with nanoparticles. (*c*) Many alloys, including AA7075, tend to solidify through columnar dendritic growth. (*d*) Suitable nanoparticles that can induce heterogeneous nucleation and promote equiaxial grain growth. (*e*) Alloys with unacceptable microstructure with large grains and periodic cracks. (*f*) Functionalizing the powder feedstock with nanoparticles produces fine equiaxed grain growth and eliminates hot cracking [83]

alloys of the Al–Si system are often characterized by anisotropy [77]. The second category of alloys is dispersion-hardened aluminium alloys, such as alloys 7XXX (AlZnCuMg), 2XXX (AlCuMg), and 6XXX (AlMgSi), commonly used as deformable alloys. They also have a wide range of crystallization temperatures at the final stages of solidification, which makes them more susceptible to hot cracking during solidification [78]. For this purpose, it becomes necessary to use ligatures for grinding grain.

In addition, due to the predominant evaporation of Zn and Mg, the dispersion-hardening alloys obtained by 3*D* printing are often characterized by a different composition in terms of the height of the deposited material. The strength of the deposited material can be significantly

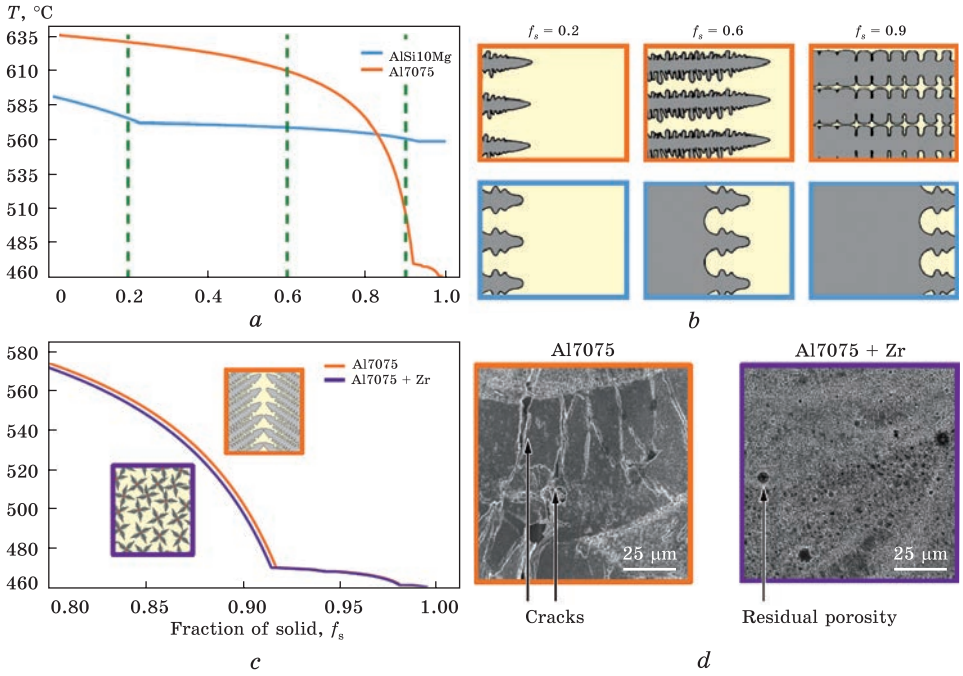


*Fig. 13.* (*a*) Solidification curves for Al7075 and AlSi10Mg alloys. (*b*) Schematic representation of solidification tops in Al7075 alloy, and bottoms in AlSi10Mg. Three panels in each row corresponding to solid fractions. (*c*) Addition of zirconium to Al7075 alloys (purple). (*d*) Scanning electron microscopy (SEM) images of Al7075 alloy microstructures without and with Zr [83]

increased by simple heat treatment with aging for these alloys, which makes them suitable for additive manufacturing. Several approaches have been taken to improve the additive processing of aluminium alloys to control the microstructure and final properties of the resulting material. In particular, the well-established literature on casting describes methods for grinding grain by modifying the composition of the alloy.

The most common method of grinding grain in the casting process is the addition of Al–Ti–B ligature to the melt. That secures the release of modifying $TiB_2$ particles, which are believed to contain an intermediate layer of $Al_3Ti$ to enhance nucleation.

By the successful use of Al–Ti–B ligature as a grain shredder in castings, they were used for alloying aluminium alloys in additive manufacturing processes, and notable grain grinding and grain growth inhibition were reported [79–81]. There is evidence that adding Zr helps to improve the resulting microstructure of aluminium alloys when using atomic layer synthesis (AS). During crystallization, particles of the $Al_3Zr$ phase are first formed in the melt, and these particles form heterogeneous nucleation centres of the primary α-Al phase. Grain grin-

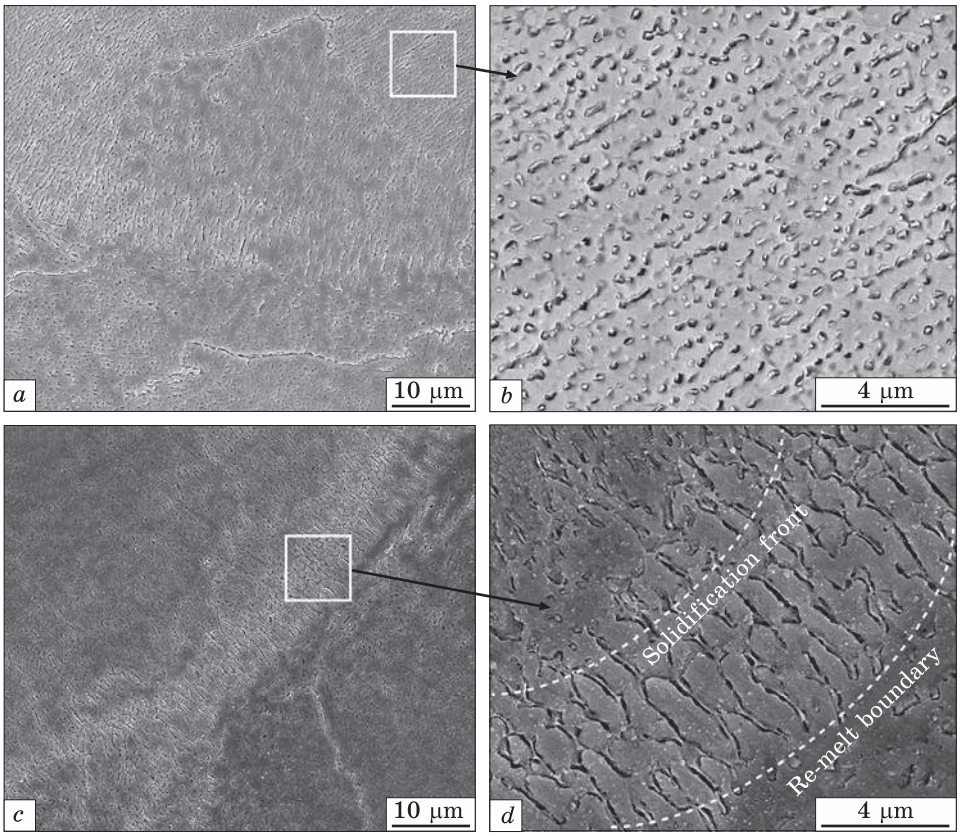


*Fig. 14*. SEM images of a dense Al–Cu–Mg alloy specimen obtained by SLM, where (*a*) and (*b*) cross section, (*c*) and (*d*) vertical section [33]

ding is also achieved by adding Sc. Like Zr, $Al_3Sc$ particles in the melt provide the formation of heterogeneous nucleation centres for primary α-Al. An additional advantage of using Sc additives in additive manufacturing processes is that it is possible to achieve a higher level of Sc solubility due to the high crystallization rate [82].

To improve the manufacturability of aluminium alloys in laser processing (LMP) and to control the microstructure and characteristics of the processed material, various approaches are used, such as grain grinding and control of the crystallization rate. Many attempts have been made to develop an alloy without fissures, and with high characteristics; however, during laser melting, cracks and pores were formed. In addition, the evaporation of Zn and Mg in the process of LMP alloy AA7075 often leads to a change in the composition of the processed material. Therefore, in the work [83], authors showed that fissure formation could be eliminated by adding germ nanoparticles during laser

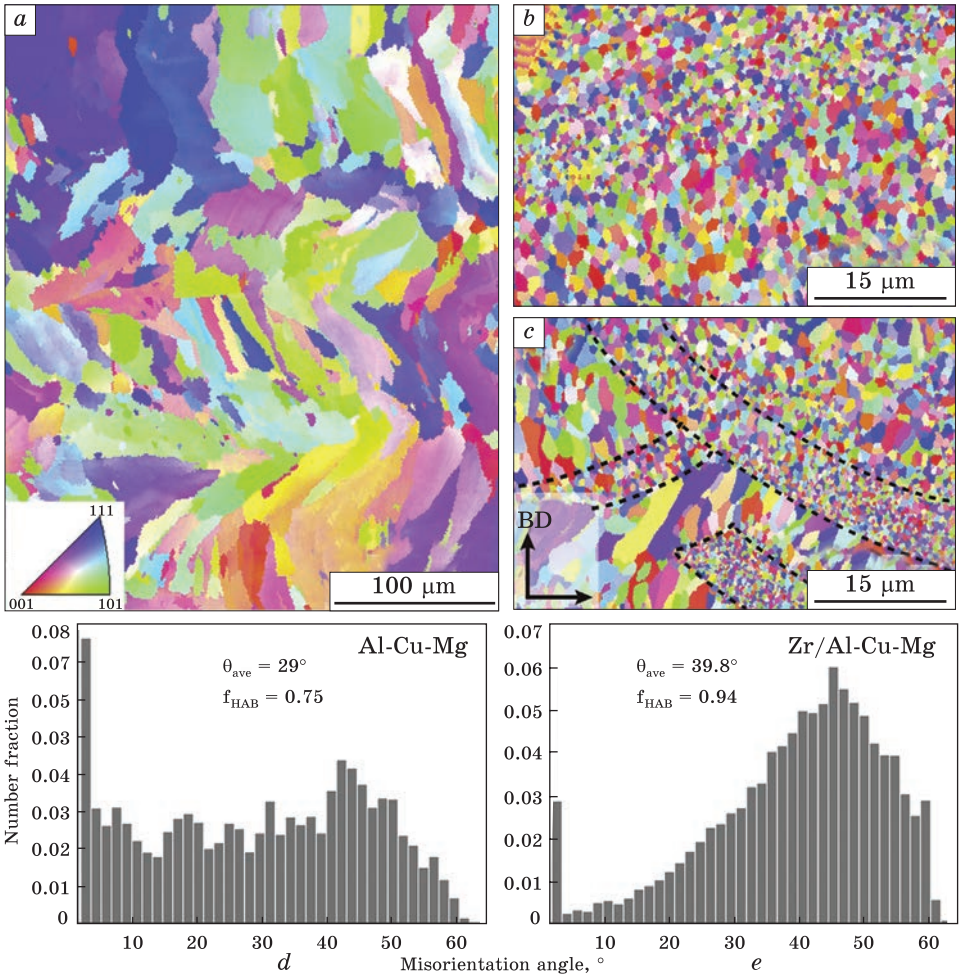


*Fig. 15*. Electron backscattered diffraction maps of Al–Cu–Mg sample obtained at scanning speed $v$ = 5 m/min (*a*), Zr/Al–Cu–Mg sample at $v$ = 5 m/min (*b*), Zr/Al–Cu–Mg sample at $v$ = 15 m/min (*c*), and distribution of disorientation angles (*d*, *e*) [52]

additive manufacturing to control solidification. Cavities and hot cracks were caused by the shrinkage of solidification of the dendritic fluid remaining between the dendritic grains [83]. Equiaxed grains, which behave like granular solids with low resistance, can reduce the influence of the remaining liquid. Small grains increase the total area of grain boundaries per unit volume, which strengthens the material and eliminates intercrystallite cracks.].

The scheme for controlling the formation of cracks during crystallization and the nucleation of new grains using grain grinders is shown in Fig. 12, *d*. Powder particles with nanoparticles with an appropriate

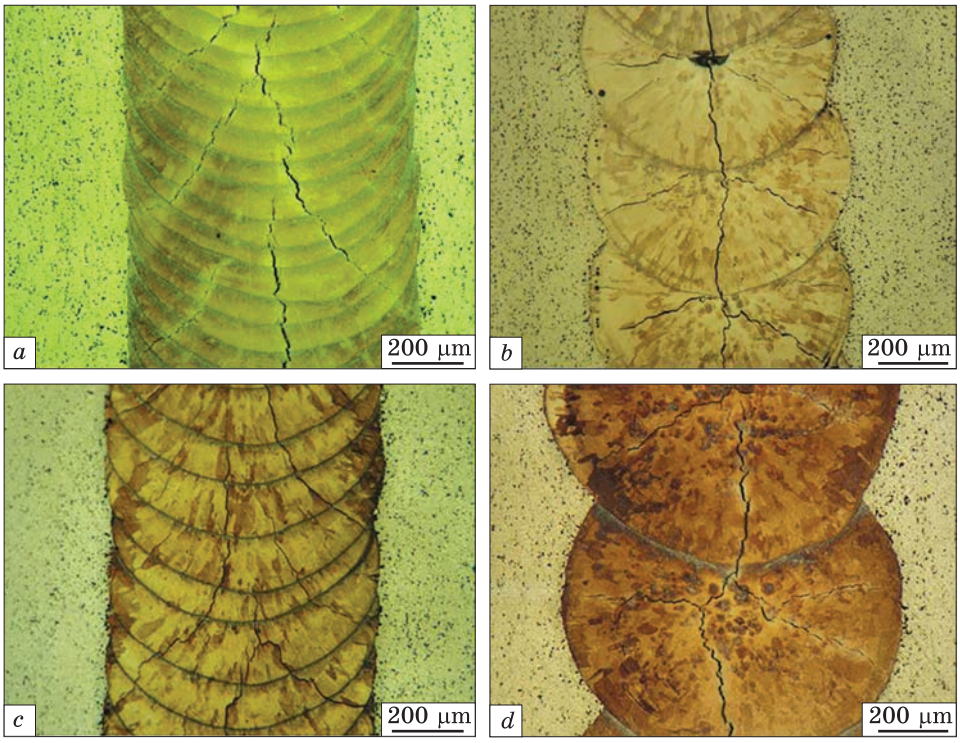


*Fig. 16*. Optical micrograph of AA2024 surface laser melting with varying degrees of overlap: 92 (*a*), 85 (*b*), 55 (*c*), and 35% (*d*) [90]

lattice (Fig. 12, *b*) lead to heterogeneous nucleation of primary equilibrium phases during the cooling of the melt bath. However, the degree of supercooling necessary to ensure uniform growth is reduced by providing a high density of heterogeneous nucleation centres with a low energy barrier in front of the solidification front. That makes it possible to obtain a fine-grained equiaxed structure, the formation of which prevents cracking and compensates for deformation under solidification conditions. This technology makes it possible to apply additive manufacturing to previously non-reproducible high-performance alloys, such as AA6061 or AA7075, with improved properties compared to currently available alloy systems [83].

The complete elimination of cracks is associated with changes in the microstructure, as shown in Fig. 13. The formation of crystallization cracks in many materials can theoretically be detected by solidification curves (Fig. 13, *a*). Alloys prone to the formation of hot fissures are characterized by wide crystallization intervals between liquidus and solidus temperatures and a sharp change in the crystallization curve at high solid-phase content. Resistance to hot cracking can be increased by

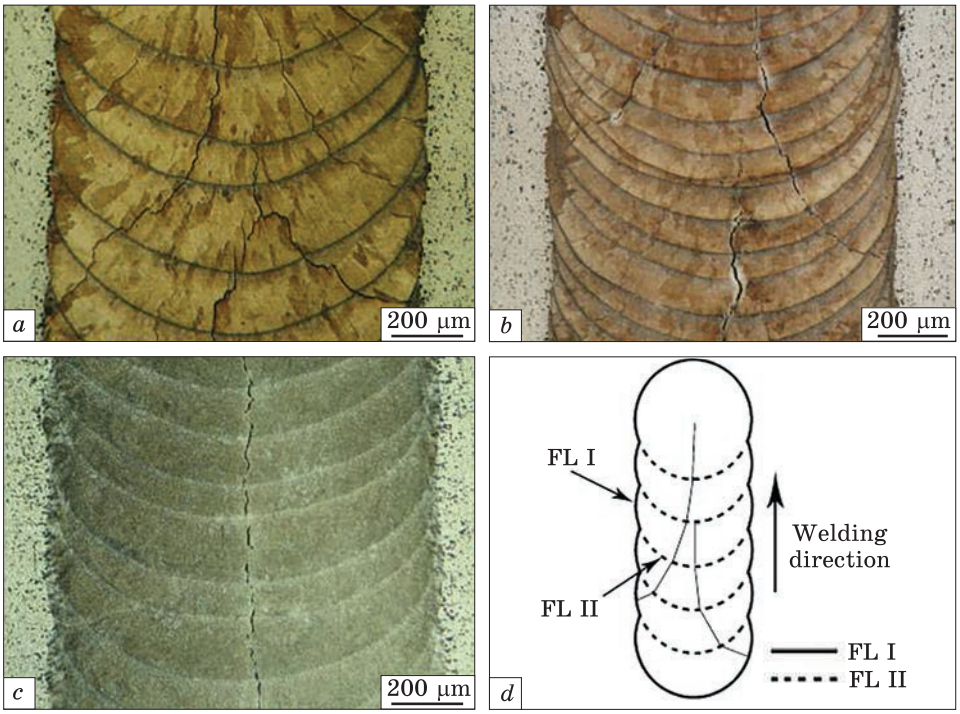


*Fig. 17*. Optical micrographs, where (*a*) without sample preheating, (*b*) with sample preheating to 350 °C, (*c*) to 250 °C, (*d*) schematic illustration of typical solidification crack morphology and different fusion lines in pulsed laser welding. FL I and FL II denote different locations of solidifications for determination of the cooling rates [93]

reducing the temperature difference between solidus and liquidus or by reducing the proportion of the solid phase. Primary inclusions of Zr promote equiaxial growth, which facilitates the perception of thermal compression deformations that occur during crystallization, because of which the alloy, contrary to popular belief, has a high resistance to hot cracks, compared with Al7075 without Zr (Fig. 13, *d*).

The most popular alloys of the Al–Cu–Mg system used in additive technologies are deformable alloys of the 2XXXX series, which have a similar composition to foundry alloys. Based on the example of the AA2024 alloy, it was shown that after selective laser spraying, the tensile strength of this alloy is approximately 400 MPa, while it is 185 MPa in the cast state [84]. As demonstrated, with an increase in energy density of more than 340 J/mm$^3$, the relative density of products exceeds 99.5%, and, as shown, microcracks and defects [85–90] thoroughly disappear. The increase in strength is explained by a significant change in the dispersion of phases, grains, and solid-solution hardening in the SLM process (Fig. 14).

As shown in Ref. [52], the addition of Zr leads to the formation of an ultrafine-grained structure, a significant reduction in hot cracks, and an increase in the tensile strength to 450 MPa. Figure 15 shows the microstructures of Al–Cu–Mg and Al–Cu–Mg–Zr alloys at different process speeds.

The high tendency of the Al–Cu–Mg alloy to crack during solidification is one of the problems of its use in laser and additive technologies. Hot (hardening) cracks occur during crystallization when the alloy passes through a temperature range, in which plasticity is very low. Cracking begins in this temperature range when thermal tensile deformations exceed the stress limit required for the crack to occur during solidification (Fig. 16) [91]. According to recent studies on the susceptibility of this material to laser cracking, high cooling rates, and rapid solidification cause cracking in aluminium alloys and other metals as well as their compounds [91, 92].

The second way to deal with crystallization cracks for this alloy is to preheat the samples before laser treatment, as shown in Fig. 17. The probability of cracking during solidification decreases with the use of preheating. Preheated examples have a lower tendency to fissure due to a lower rate of induced deformation rather than due to slower filler feed rate. Since higher local deformation and lower fluid flow rates play a significant role in crack propagation, effective preheating cannot stop crack propagation along the fusion lines between pulses. On the other hand, the expansion of previous fissures from previously loaded pulses can prevent the occurrence of new cracks in subsequent pulses [93].

## 4. Conclusions

This article reviews, analyses, and, therefore, contributes to further studying of alloys treated with laser melting to illuminate new alloys without defects and improved mechanical properties. There are obvious applications of high-strength aluminium alloys for SLM, and for this, there are more and more ways to develop deformable alloys that are strengthened by aging. However, suitable alloys are difficult to process because they are prone to cracking. The most common types of aging-hardened alloys were also discussed to properly evaluate potential alloys.

REFERENCES

1. W.E. King, A.T. Anderson, R.M. Ferencz, N.E. Hodge, C. Kamath, S.A. Khairallah, and A.M. Rubenchik, *Appl. Phys. Rev.*, **2**: 41304 (2015); https://doi.org/10.1063/1.4937809
2. A. Kolesnikov, R. Fediuk, S. Klyuev, L. Sabitov, T. Zhuniskaliyev, B. Kelamanov, D. Yessengaliev, A. Yerzhanov, and O. Kolesnikova, *Materials*, **15**: 2584 (2022); https://doi.org/10.3390/ma15072584

3. I.E. Volokitina, *J. Chem. Technol. Metall.*, **55**, No. 2: 479 (2020).
4. X.P. Li, C.W. Kang, H. Huang, L.C. Zhang, and T.B. Sercombe, *Mater. Sci. Eng. A*, **606**: 370 (2014); https://doi.org/https://doi.org/10.1016/j.msea.2014.03.097
5. S. Kenzari, D. Bonina, J.-M. Dubois, and V. Fournйe, *J. Mater. Process. Technol.*, **214**: 3108 (2014); https://doi.org/https://doi.org/10.1016/j.jmatprotec.2014.07.011
6. A. Donayev, A. Kolesnikov, S. Shapalov, B. Sapargaliyeva, and G. Ivakhniyuk, *News of the National Academy of Sciences of the Republic of Kazakhstan, Series of Geology and Technical Sciences*, **55** (2022).
7. J. Majumdar and I. Manna, *Laser Processing of Materials*, **28**: 495 (2003); https://doi.org/10.1007/BF02706446
8. O. Kolesnikova, S. Syrlybekkyzy, R. Fediuk, A. Yerzhanov, R. Nadirov, A. Utelbayeva, A. Agabekova, M. Latypova, L. Chepelyan, I. Volokitina, N. Vatin, A. Kolesnikov, and M. Amran, *Materials,* **15**: 6980 (2022); https://doi.org/10.3390/ma15196980
9. W.M. Steen and J. Mazumder, *Laser Material Processing* (London: Springer: 2010); https://doi.org/10.1007/978-1-84996-062-5
10. I. Volokitina, E. Siziakova, R. Fediuk, and A. Kolesnikov, *Materials*, **15**, No. 14: 3975 (2022); https://doi.org/10.3390/ma15144930
11. C.Y. Yap, C.K. Chua, Z.L. Dong, Z.H. Liu, D.Q. Zhang, L.E. Loh, and S.L. Sing, *Appl. Phys. Rev.*, **2**, No. 4: 041101 (2015); https://doi.org/10.1063/1.4935926
12. W.T. Carter and M.G. Jones, *Proceeding SFF Symp.* (1993), vol. **51**.
13. I.J. Polmear, *Light Alloys (Fourth Edition): From Traditional Alloys to Nanocrystals* (Oxford: Butterworth-Heinemann: 2005), p. 1; https://doi.org/10.1016/B978-075066371-7/50005-0
14. C.C. Ng, M.M. Savalani, H.C. Man, and I. Gibson, *Virtual Phys. Prototyp.*, **5**: 13 (2010); https://doi.org/10.1080/17452751003718629
15. B. Zhang, H. Liao, and C. Coddet, *Mater. Des.*, **34**: 753 (2012); https://doi.org/10.1016/j.matdes.2011.06.061
16. K. Wei, M. Gao, Z. Wang, and X. Zeng, *Mater. Sci. Eng. A*, **611**: 212 (2014); https://doi.org/10.1016/j.msea.2014.05.092
17. V. Manakari, G. Parande, and M. Gupta, *Metals*, **7**, No. 1: 2 (2017); https://doi.org/10.3390/met7010002
18. A.B. Spierings, K. Dawson, K. Kern, F. Palm, and K. Wegener, *Mater. Sci. Eng. A*, **701**: 264 (2017); https://doi.org/10.1016/j.msea.2017.06.089
19. N.T. Aboulkhair, N.M. Everitt, I. Maskery, I. Ashcroft, and C. Tuck, *MRS Bull.*, **42**: 311 (2017); https://doi.org/10.1557/mrs.2017.63
20. D. Koutny, D. Palousek, O. Koukal, T. Zikmund, L. Pantelejev, and F. Dokoupil, *Lasers Manuf. Conf.*, 2015 (2015).
21. S. Lezhnev, A. Naizabekov, E. Panin, and I. Volokitina, *Procedia Engineering*, **81**: 15 (2014); https://doi.org/10.1016/j.proeng.2014.10.180
22. A. Naizabekov, S. Lezhnev, E. Panin, I. Volokitina, A. Arbuz, T. Koinov, and I. Mazur, *J. Mater. Eng. Perform.*, **28**: 200 (2019); https://doi.org/10.1007/s11665-018-3790-z

23. T. Amine, J.W. Newkirk, and F. Liou, *Appl. Therm. Eng.*, **73**: 500 (2014); https://doi.org/10.1016/j.applthermaleng.2014.08.005
24. S. Lezhnev, A. Naizabekov, A. Volokitin, and I. Volokitina, *Procedia Engineering*, **81**: 1505 (2014); https://doi.org/10.1016/j.proeng.2014.10.181
25. L. Parimi, R. Aswathanarayanaswamy, D. Clark, and M. Attallah, *Mater. Charact*. **89** (2014); https://doi.org/10.1016/j.matchar.2013.12.012
26. S. Bhattacharya, G. Dinda, A. Dasgupta, and J. Mazumder, *J. Mater. Sci.*, **49**: 2415 (2014); https://doi.org/10.1007/s10853-013-7883-7
27. G. Dinda, A. Dasgupta, S. Bhattacharya, H. Natu, B. Dutta, and J. Mazumder, *Metall. Mater. Trans. A*, **44**: 2233(2012); https://doi.org/10.1007/s11661-012-1560-3
28. T. DebRoy, H.L. Wei, J.S. Zuback, T. Mukherjee, J.W. Elmer, J.O. Milewski, A.M. Beese, A. Wilson-Heid, A. De, and W. Zhang, *Prog. Mater. Sci.*, **92**: 112 (2018); https://doi.org/10.1016/j.pmatsci.2017.10.001
29. I. Volokitina, N. Vasilyeva, R. Fediuk, and A. Kolesnikov, *Materials*, **15**: 3975 (2022); https://doi.org/10.3390/ma15113975
30. A. Volokitin and A. Naizabekov, *J. Chem. Technol. Metallurgy*, **58**, No. 4: 806 (2023); https://doi.org/10.3390/ma15144930
31. L.N. Carter, C. Martin, P.J. Withers, and M.M. Attallah, *J. Alloys Compd.*, **615**: 338 (2014); https://doi.org/10.1016/j.jallcom.2014.06.172
32. Z. Wang, R. Ummethala, N. Singh, S. Tang, C. Suryanarayana, J. Eckert, and K.G. Prashanth, *Materials*, **13**, No. 20: 4564 (2020); https://doi.org/10.3390/ma13204564
33. H. Zhang, H. Zhun, T. Qi, Z. Hu, and X. Zeng, *Mater. Sci. Eng. A*, **656**: 47 (2016); https://doi.org/10.1016/j.msea.2015.12.101
34. D. Bayoumy, D. Schliephake, S. Dietrich, X.H. Wu, Y.M. Zhu, and A.J. Huang, *Mater. Des.*, **198**: 15 (2021); https://doi.org/10.1016/j.matdes.2020.109317
35. T. Amine, J. Newkirk, and F. Liou, *Appl. Therm. Eng.*, **73**, No. 1: 500 (2014); https://doi.org/10.1016/j.applthermaleng.2014.08.005
36. I. Volokitina, *Metal Science and Heat Treatment*, **62**: 253 (2020); https://doi.org/10.1007/s11041-020-00544-x
37. B. Zhang, L. Dembinski, and C. Coddet, *Mater. Sci. Eng. A*, **584**: 21 (2013); https://doi.org/10.1016/j.msea.2013.06.055
38. M. Doubenskaia, M. Pavlov, and Y. Chivel, *Key Eng. Mater*, **437**: 458 (2010); https://doi.org/10.4028/www.scientific.net/KEM.437.458
39. Y. Gao, J. Xing, J. Zhang, N. Luo, and H. Zheng, *Optik*, **119**: 618 (2008); https://doi.org/10.1016/j.ijleo.2007.01.010
40. I.E. Volokitina, *J. Chem. Technol. Metallurgy,* **57**: 631 (2022).
41. D. Hu and R. Kovacevic, *J. Mach. Tools Manuf.*, **43**: 51 (2003); https://doi.org/10.1016/S0890-6955(02)00163-3
42. T. Mukherjee, W. Zhang, and T. Debroy, *Comput. Mater. Sci.*, 126 (2017); https://doi.org/10.1016/j.commatsci.2016.10.003

43. T.G. Spears and S.A. Gold, *Integr. Mater. Manuf. Innov.*, **5**: 16 (2016); https://doi.org/10.1186/s40192-016-0045-4
44. S. Katayama, *Weld. Int.*, **14**: 939 (2000); https://doi.org/10.1080/09507110009549297
45. Y. Shi, K. Yang, S.K. Kairy, F. Palm, X. Wu, and P.A. Rometsch, *Mater. Sci. Eng. A*, **732**: 41 (2018); https://doi.org/10.1016/j.msea.2018.06.049
46. C. Galy, E. Le Guen, E. Lacoste, and C. Arvieu, *Addit. Manuf.*, **22**: 165 (2018); https://doi.org/10.1016/j.addma.2018.05.005
47. M. Karg, B. Ahuja, S. Kuryntsev, A. Gorunow, and M. Schmidt, *Int. Conf. 25th Solid Freeform Fabrication Symposium in Austin* (Texas: 2014); https://doi.org/10.13140/RG.2.2.11672.85763
48. K. Karami, A. Blok, L. Weber, S.M. Ahmadi, R. Petrov, K. Nikolic, E.V. Borisov, S. Leeflang, C. Ayas, A.A. Zadpoor, M. Mehdipour, E. Reinton, and V.A. Popovich, *Addit. Manuf.*, **36**: 101433 (2020); https://doi.org/10.1016/j.addma.2020.101433
49. W.E. King, A.T. Anderson, R.M. Ferencz, N.E. Hodge, C. Kamath, S.A. Khairallah, and A.M. Rubenchik, *Appl. Phys. Rev.*, **2**: 41304 (2015); https://doi.org/10.1063/1.4937809
50. T. Kimura and T. Nakamoto, *Mater. Des.*, **89**: 1294 (2016); https://doi.org/10.1016/j.matdes.2015.10.065
51. C. Weingarten, D. Buchbinder, N. Pirch, W. Meiners, K. Wissenbach, and R. Poprawe, *J. Mater. Process. Technol.*, **221**: 112 (2015); https://doi.org/10.1016/j.jmatprotec.2015.02.013
52. H. Zhang, H. Zhu, X. Nie, J. Yin, Z. Hu, and X. Zeng, *Scr. Mater.*, **134**: 6 (2017); https://doi.org/10.1016/j.scriptamat.2017.02.036
53. T. Delgado, L. Gonza, F.J. Botana, and J.M. Sa, *Appl. Surf. Sci.*, **255**: 9512 (2009); https://doi.org/10.1016/j.apsusc.2009.07.081
54. X. Cao, B. Wallace, C. Poon, and J.-P. Immarigeon, *Mater. Manuf. Process.*, **18**, No. 1: 1 (2003); https://doi.org/10.1081/AMP-120017586
55. A.V. Volokitin, E.A. Panin, M.A. Latypova, and S.S. Kassymov, *Eurasian Physical Technical Journal*, **19**, No. 1 (39): 73 (2022); https://doi.org/10.31489/2022No1/73-77
56. 56. G.K. Sigworth, Hot tearing of metals, *AFS Transactions*, 1053 (2002).
57. 57. D.G. Eskin and L. Katgerman, *Metall. Mater. Trans. A*, **38**: 1511 (2007); https://doi.org/10.1007/s11661-007-9169-7
58. M.L. Montero Sistiaga, R. Mertens, B. Vrancken, X. Wang, B. Van Hooreweder, J.P. Kruth, and J. Van Humbeeck, *J. Mater. Process. Technol.*, **238**: 437 (2016); https://doi.org/10.1016/j.jmatprotec.2016.08.003
59. H.L. Wei, J.W. Elmer, and T. DebRoy, *Acta Mater.*, **126**: 413 (2017); https://doi.org/10.1016/j.actamat.2016.12.073
60. H.L. Wei, J.W. Elmer, and T. Debroy, Origin of grain orientation during solidification of an aluminum alloy, *Acta Mater.*, **115**: 123 (2016); https://doi.org/10.1016/j.actamat.2016.05.057
61. Y. Lee, M. Nordin, S.S. Babu, and D.F. Farson, Effect of fluid convection on dendrite arm spacing in laser deposition, *Metall. Mater. Trans. B*, **45**: 1520 (2014); https://doi.org/10.1007/s11663-014-0054-7
62. S. Chen, X. Zhan, Y. Zhao, Y. Wu, and D. Liu, Influence of laser power on grain size and tensile strength of 5a90 Al–Li alloy T-joint fabricated by dual laser-

beam bilateral synchronous welding, *Met. Mater. Int.*, **27**: 1671 (2021); https://doi.org/10.1007/s12540-019-00538-2
63. R. Rajan, P. Kah, B. Mvola, and J. Martikainen, *Reviews on Advanced Materials Science*, **44**: 383 (2016).
64. A.A.Y. Al-qenaei, *Fusion Welding Techniques*, **6**: 78 (2016).
65. I.N. Shiganov, S.V. Shakhov, and A.A. Kholopov, Lazernaya Svarka Alyuminievykh Splavov Aviatsionnogo Naznacheniya [Laser Welding of Aircraft Aluminium Alloys], *Bulletin of N.E. Bauman Moscow State Technical University* (2012) (in Russian).
66. T.M. Radchenko, V.A. Tatarenko, H. Zapolsky, and D. Blavette, Statistical-Thermodynamic Description of the Order–Disorder Transformation of $D0_{19}$-Type Phase in Ti–Al Alloy, *J. Alloys Compd.*, **452**, No. 1: 122 (2008); https://doi.org/10.1016/j.jallcom.2006.12.149
67. D.S. Leonov, T.M. Radchenko, V.A. Tatarenko, and Yu.A. Kunitsky, Kinetics Parameters of Atomic Migration and Diffuse Scattering of Radiations within the F.C.C.-Ni–Al Alloys, *Defect and Diffusion Forum*, **273–276**: 520 (2008); https://doi.org/10.4028/www.scientific.net/DDF.273-276.520
68. T.M. Radchenko, O.S. Gatsenko, V.V. Lizunov, and V.A. Tatarenko, Martensitic $\alpha''$-$Fe_{16}N_2$-Type Phase of Non-Stoichiometric Composition: Current Status of Research and Microscopic Statistical-Thermodynamic Model, *Progress in Physics of Metals*, **21**, No. 4: 580 (2020); https://doi.org/10.15407/ufm.21.04.580
69. V.A. Tatarenko, S.M. Bokoch, V.M. Nadutov, T.M. Radchenko, and Y.B. Park, Semi-Empirical Parameterization of Interatomic Interactions and Kinetics of the Atomic Ordering in Ni–Fe–C Permalloys and Elinvars, *Defect and Diffusion Forum*, **280–281**: 29 (2008); https://doi.org/10.4028/www.scientific.net/DDF.280-281.29
70. V.A. Tatarenko and T.M. Radchenko, The Application of Radiation Diffuse Scattering to the Calculation of Phase Diagrams of F.C.C. Substitutional Alloys, *Intermetallics*, **11**, Nos. 11–12: 1319 (2003); https://doi.org/10.1016/S0966-9795(03)00174-2
71. I.M. Melnyk, T.M. Radchenko, and V.A. Tatarenko, Semi-Empirical Parameterization of Interatomic Interactions, Which Is Based on Statistical-Thermodynamic Analysis of Data on Phase Equilibriums in B.C.C.-Fe–Co Alloy. I. Primary Ordering, *Metallofizika i Noveishie Tekhnologii,* **32**, No. 9: 1191 (2010).
72. P. Kah, R. Rajan, J. Martikainen, R. Suoranta, Investigation of weld defects in friction-stir welding and fusion welding of aluminium alloys, *Int. J. Mech. Mater. Eng.*, **10**: 1 (2015); https://doi.org/10.1186/s40712-015-0053-8
73. S. Kou, Solidification and liquation cracking issues in welding, *JoM*, **55**: 37 (2003); https://doi.org/10.1007/s11837-003-0137-4
74. A. Ramirez, J. Graciano-Uribe, D. Hincapie, and E. Torres, Segregation effect on solidification cracking in spot welding of the 6xxx aluminum, *Eng. Trans.*, **68**: 417 (2020); https://doi.org/10.24423/EngTrans.1185.20201120
75. J.F. Lancaster, Non-ferrous metals, *Metallurgy of Welding* (Woodhead Publishing: 1999), p. 353; https://doi.org/10.1533/9781845694869.353
76. C. Huang, G. Cao, and S. Kou, *Sci. Technol. Weld. Join.*, **9**, No. 2: 149 (2004); https://doi.org/10.1179/136217104225017071

77. Y.C. Lee, A.K. Dahle, D.H. StJohn, and J.E.C. Hutt, *Mater. Sci. Eng. A*, **259**: 43 (1999);
https://doi.org/10.1016/S0921-5093(98)00884-3
78. F. Wang, D. Qiu, Z.-L. Liu, J.A. Taylor, M.A. Easton, and M.-X. Zhang, *Acta Mater.*, **61**: 5636 (2013);
https://doi.org/10.1016/j.actamat.2013.05.044
79. Y.K. Xiao, Z.Y. Bian, Y. Wu, G. Ji, Y.Q. Li, M.J. Li, Q. Lian, Z. Chen, A. Addad, and H.W. Wang, *J. Alloys Compd.*, **798**: 644 (2019);
https://doi.org/10.1016/j.jallcom.2019.05.279
80. X. Wen, Q. Wang, Q. Mu, N. Kang, S. Sui, H. Yang, X. Lin, and W. Huang, *Mater. Sci. Eng. A*, **745**: 319 (2019);
https://doi.org/10.1016/j.msea.2018.12.072
81. I.E. Volokitina, A.V. Volokitin, and E.A. Panin, Martensitic Transformations in Stainless Steels, *Progress in Physics of Metals*, **23**, No. 4: 684 (2022);
https://doi.org/10.15407/ufm.23.04.684
82. Y. Shi, P. Rometsch, K. Yang, F. Palm, and X. Wu, *Mater. Lett.*, **196**: 347 (2017);
https://doi.org/10.1016/j.matlet.2017.03.089
83. J.H. Martin, B.D. Yahata, J.M. Hundley, J.A. Mayer, T.A. Schaedler, and T.M. Pollock, *Nature*, **549**: 365 (2017);
https://doi.org/10.1038/nature23894
84. H. Zhang, H. Zhu, T. Qi, Z. Hu, and X. Zeng, *Mater. Sci. Eng. A*, **656**: 47 (2016);
https://doi.org/10.1016/j.msea.2015.12.101
85. V.B. Molodkin, S.I. Olikhovskii, S.V. Dmitriev, A.I. Nizkova, and V.V. Lizunov, *Acta Crystallographica Section A: Foundations and Advances*, **76**: 45 (2020);
https://doi.org/10.1107/S2053273319014281
86. V.B. Molodkin, S.I. Olikhovskii, S.V. Dmitriev, and V.V. Lizunov, *Acta Crystallographica Section A: Foundations and Advances*, **77**: 433 (2021);
https://doi.org/10.1107/S2053273321005775
87. S.V. Lizunova, V.B. Molodkin, B.V. Sheludchenko, and V.V. Lizunov, *Metallofizika i Noveishie Tekhnologii*, **35**, No. 11: 1585 (2013).
88. E.G. Len, I.M. Melnyk, S.P. Repetsky, V.V. Lizunov, and V.A. Tatarenko, *Materialwissenschaft und Werkstofftechnik*, **42**, No. 1: 47 (2011);
https://doi.org/10.1002/mawe.201100729
89. S.P. Repetsky, T.S. Len, and V.V. Lizunov, *Metallofizika i Noveishie Tekhnologii*, **28**, No. 9: 1143 (2006).
90. S.P. Repetsky, E.G. Len, and V.V. Lizunov, *Metallofizika i Noveishie Tekhnologii*, **28**, No. 8: 989 (2006).
91. M. Sheikhi, F.M. Ghaini, M.J. Torkamany, and J. Sabbaghzadeh, *Sci. Technol. Weld. Join.*, **14**: 161 (2009);
https://doi.org/10.1179/136217108X386554
92. Yu.Ya. Meshkov, G.P. Zimina, and N.M. Stetsenko, Nature of the Brittleness of Metals, *Progress in Physics of Metals*, **23**, No. 4: 744 (2022);
https://doi.org/10.15407/ufm.23.04.744
93. M. Sheikhi, F. Malek Ghaini, and H. Assadi, *Sci. Technol. Weld. Join.*, **19**, No. 3: 250 (2014);
https://doi.org/10.1179/1362171813Y.0000000190

Received 08.03.2023;
in final version, 05.08.2023

*М.А. Латипова*[1], *С.Л. Кузьмін*[2], *А.С. Єржанов*[1]
[1] Карагандинський індустріяльний університет,
560пр. Республіки, 30, 101400 Темиртау, Казахстан
[2] Руднеський індустріяльний інститут,
вул. 50 років Жовтня, 38, 111500 Рудний, Казахстан

## ВПЛИВ ПАРАМЕТРІВ ПРОЦЕСУ СЕЛЕКТИВНОГО ЛАЗЕРНОГО ТОПЛЕННЯ НА ФОРМУВАННЯ МІКРОСТРУКТУРИ

Останнім часом бурхливо розвиваються адитивні технології одержання виробів методом лазерного топлення порошків. Але такі технології висувають підвищені вимоги до властивостей стопів, застосовуваних для виготовлення деталів. Технології лазерного топлення є перспективним напрямом у розробленні виробів із металів завдяки ряду переваг, таких як: (1) можливість виготовлення деталів складної форми з внутрішніми порожнинами та тонкими перегородками, (2) значна економія матеріалу за рахунок точного виготовлення деталю заданої форми за комп'ютерним моделем, що не вимагає застосування наступних звичайних операцій токарного, фрезерного оброблення й оброблення різанням, (3) досягнення вищого рівня механічних властивостей за допомогою підвищених швидкостей охолодження у порівнянні зі стандартними технологіями через формування дисперсної структури.

**Ключові слова:** адитивні технології, порошкова металургія, селективне лазерне топлення, мікроструктура, керування мікроструктурою, термічне оброблення.